UC San Diego
UC San Diego Previously Published Works

Title
Assessment of embedded fiber Bragg gratings for structural health monitoring of composites

Permalink
https://escholarship.org/uc/item/67q6w8vm

Journal
Structural Health Monitoring, 16(3)

ISSN
1475-9217

Authors
Yeager, Mike
Todd, Michael
Gregory, William
et al.

Publication Date
2017-05-01

DOI
10.1177/1475921716665563

Peer reviewed

IWSHM 2015: Assessment of Embedded Fiber Bragg Gratings for Structural Health Monitoring Of Composites

Mike Yeager[1], Michael Todd[1], William Gregory[2], Chris Key[2]

[1]Department of Structural Engineering, University of California San Diego, La Jolla CA 92093 USA; email: mdtodd@ucsd.edu
[2]Applied Physical Sciences, Groton, CT 06340 USA

ABSTRACT

This work provides a systems-level investigation into the use of embedded fiber Bragg grating (FBG) optical sensors as a viable sensing architecture for the structural health monitoring (SHM) of composite structures. The practical aspects of the embedding process are documented for both carbon fiber reinforced polymer (CFRP) and glass fiber reinforced polymer (GFRP) structures manufactured by both oven vacuum bag (OVB) and vacuum assisted resin transfer (VARTM) processes. Initially, embedded specimens were subject to long-term water submersion to verify performance in an underwater environment. Static load tests of the specimens were performed to both cross-compare results and to compare to structural finite element analysis (FEA) results. A larger, more complex jointed specimen was also fabricated with a fully embedded sensor network of FBGs and subjected to incrementally-induced bearing damage. Using commercially available interrogation hardware, a damage detection SHM algorithm was developed and deployed. The results permit statistically precise detection of low levels of connection damage in the composite specimen.

KEYWORDS

Fiber Bragg Gratings, Bearing Damage, Embedded Sensors, Composites, Feature Extraction

INTRODUCTION

Because of their high specific strength and stiffness, corrosion resistance, and ability to be molded into complex shapes, fiber reinforced polymer (FRP) composite structures are gaining more prevalence in marine[1, 2] and aerospace[3, 4] industries. The performance benefits from composites—typically, weight reduction with increased strength, corrosion resistance, and improved thermal and acoustic properties—are challenged by a host of failure modes (delamination, disbonding, fiber breakage, matrix cracking, etc.) whose initiation and progression are not well understood and often cannot be detected by visual inspection. Although substantive research advances have been made towards damage analysis and modeling of the aforementioned failure modes in composites[5-10], research and development of structural health monitoring (SHM) systems are still needed for the purposes of performance/operations optimization,

maintenance planning, and overall life cycle cost reduction.

Structural health monitoring may be defined the process of implementing a decision-enabling damage detection strategy, and it necessarily involves acquiring data while in service, extracting damage-sensitive features from the data, and assessing the condition of the structure via statistical hypothesis testing.[11] Although many sensing modalities have been employed in the literature[12-16], fiber optic sensors—and in particular fiber Bragg gratings (FBGs)—have gained considerable traction as an attractive sensing option because they are light-weight, corrosion-resistant, impermeable to liquid absorption, immune to electromagnetic interference, do not provide a spark source, and are embeddable in composites.[17-20] Although there have been many segmented investigations into the use of embedded FBGs in the health monitoring of composites, there has not been many systems-level studies that explore the entirety of the process from embedment during manufacture to statistical decision making during operation. This paper consists of three phases to fully explore the process:

- **Phase I**: Assessment of FBG performance after prolonged water submersion for both embedded and surface mounted FBGs.
- **Phase II**: Comparison between embedded sensor performance for OVB and VARTM manufacturing techniques
- **Phase III**: Damage detection test on a larger bolted specimen subjected to increasing levels of bearing damage and interrogated during simulated random operational loadings

Testing in Phase I consisted of static load/deflection curve comparisons between "coupon-sized" test specimens and FE models. Assessments were conducted for both surface mounted (with non-marine epoxy) and embedded FBG sensor performance after substantial water exposure. Phase II employed the same testing methodology as Phase I, but with the intent of exploring the effects of the manufacturing process on sensor performance. Finally, Phase III assesses the viability of embedded FBGs in a damage detection scenario for a bolted composite specimen. The primary contribution of this paper is to assess the robustness of embedded FBGs during an end-to-end process of manufacturing and deployment, and to subsequently demonstrate their use as part of a practical SHM composite damage assessment application.

PHASE I: WETTED ENVIRONMENT TESTING

One of the attractive features of fiber optic sensors as a sensing architecture, especially for marine and submarine applications, is liquid absorption impermeability. To test the robustness of this favorable characteristic, composite specimens were tested after prolonged submersion in water.

Test Article Manufacture

The test articles were fabricated with the GURIT Sprint WRE850T/ST94 material system and designed to a nominal thickness of 0.8 in., using 30 warps-parallel plies of material. An L-shaped mold was constructed on the mold table as shown in Figure 1

(left). This allowed the plies to be stacked up consistently through the thickness and to maintain panel "squareness". During the lay-up process, the sensors were located at specific plies internal to the overall panel. Locations for the sensors were marked using permanent markers, and the fiber optic sensors were then placed at the marked location. Micron Optics os1200™ FBG arrays were used for the internal sensors. Once the internal sensors were positioned and secured, the next ply was laid down and build-up to the overall laminate thickness continued. Once all of the plies were laid down, the test articles were prepared for vacuum bagging and subsequent cure.

A key feature in the bagging and curing of the test articles was the attention to the fiber optic cable leads for the internal sensors. As part of the cure cycle, the reinforcement undergoes significant consolidation, requiring special attention for the ingress/egress of the array leads. To accommodate this consolidation for the embedded internal fiber optic sensors, extra steps were necessary during the set-up of the panel cure to help ensure that the optical lead to the sensors survived the cure. First, in order to avoid a kink in the lead as it exited the side of the panel, it was necessary to place a landing (vacuum bag sealer was used to build up a landing) to support the wire. Figure 1 (middle) shows the array lead support for one specimen prior to applying the vacuum bag. Second, Teflon tape was used to provide a resin barrier at the actual ingress/egress point to avoid infiltration into the array connectors, since the entire connector system had to be placed inside the vacuum bags in order to achieve the required vacuum. After laying up each of the panels, the uncured specimens were placed on a mold table with a G10 caul plate placed atop each specimen to provide a smooth bag side surface. Figure 1 (right) shows each of the panels on the mold table during the bagging process.
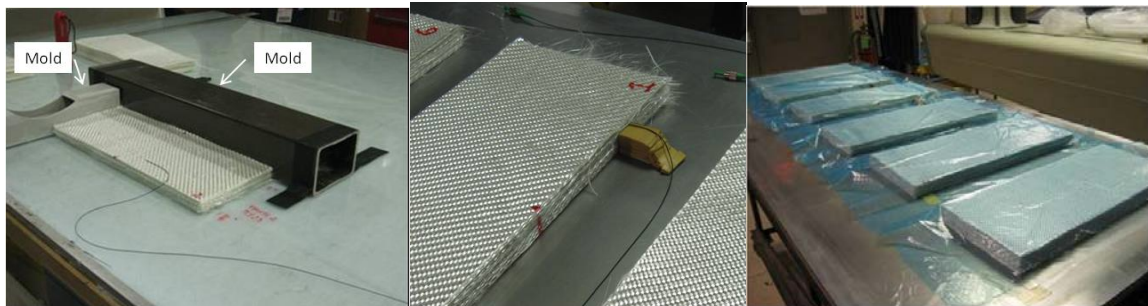

Figure 1: (left) mold set-up; (middle) sacrificial material for lead support; (right) test panels in vacuum bag

In addition to the FBG embedded arrays, surface mounted arrays were also installed on select panels after the cure process using Micron Optics os1200^{TM} and os3200^{TM} arrays. The surface installation involved lightly sanding the panel in the sensor locations and cleaning with acetone to prepare a clean and uniform bonding substrate. After the fiber was placed appropriately in its designated location and temporarily fixed with tape, a two-phase mixed strain gage epoxy was applied along the 2.54 in. gage length of the photo-etched sensing portion of each fiber. The epoxy was then allowed to cure for 12 hours.

Specimen Testing

Three-point bend testing was selected to be the primary initial verification approach. A support spacing of 16 in. for the 0.8 in. thick panel was selected to allow the first mode of failure to be matrix cracking followed by fiber failure. This support distance would also preclude large deflection interaction. The test machine used for these tests is shown in Figure 2. As shown in the figure, the bottom supports for the fixture consisted of 1.5 in. diameter rounds spaced 16 in. apart. The loading head was also a 1.5 in. round directly centered between the supports. To accommodate the "wet" testing, a plexiglass aquarium-type structure was fabricated, incorporating the end fixtures. This allowed for both dry and "wet" testing to be conducted simply by filling up the aquarium and subsequently draining the aquarium. A Micron Optics SM170 Fiber Optic Interrogator was used as both the broadband light source and light receiver. Micron Optics' Enlight software was used to track the peak wavelength shifts on a Dell laptop computer.
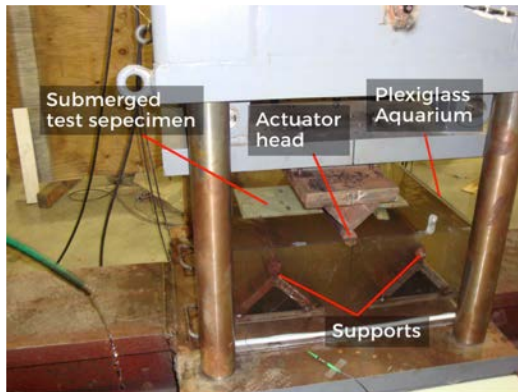

Figure 2: Bending test fixture, including aquarium for wetted environment

After the post-fabrication cure, it was determined that all internal sensors functioned properly, withstanding the cure temperature of 185°F for 12 hours under a full vacuum. The general testing procedure involved 6 total panels, some of which were instrumented with embedded gages and others with surface-mounted gages. Most panels were elastically loaded, and a subset was gradually loaded to failure. From all the test panels, Panel 2 was selected as an example to demonstrate the performance of the embedded fiber optic sensors in a dry environment. Panel 2 contained two internal sensors installed 7 plies from the compression side of the panel. Two elastic runs were conducted on this panel up to 5000 lbs.; these tests were followed by a test to failure of 18,800 lbs. The internal sensors survived the fabrication and were able to provide strain response as indicated in Figure 3. The figure also plots predicted strain readings from a surrogate FE model of the test specimens and communicates strong agreement between the model and the empirical strain data.
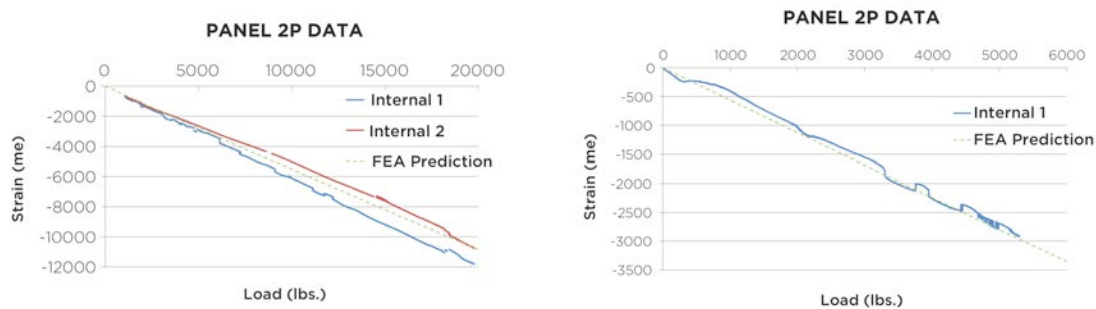

Figure 3: Embedded sensor performance to failure (left) and within elastic range (right)

During testing, some "peak hopping" occurred, which led to the observed discontinuous strain histories seen in Figure 3. These are a consequence of the data acquisition software's failure to accurately track central FBG reflection peaks; under load, FBGs may become chirped (suffer non-negligible strain gradients over the sensing length), which lead to overall reflection peak broadening and distortion. This effect is enhanced for embedded FBGs, where microstructure/resin interaction can lead to micro-constriction and micro-bending in the fiber. Peak hopping and micro-bending will be discussed later in the paper along with potential corrective techniques.

PANEL 5
DRY VS. 7 WEEK SOAK
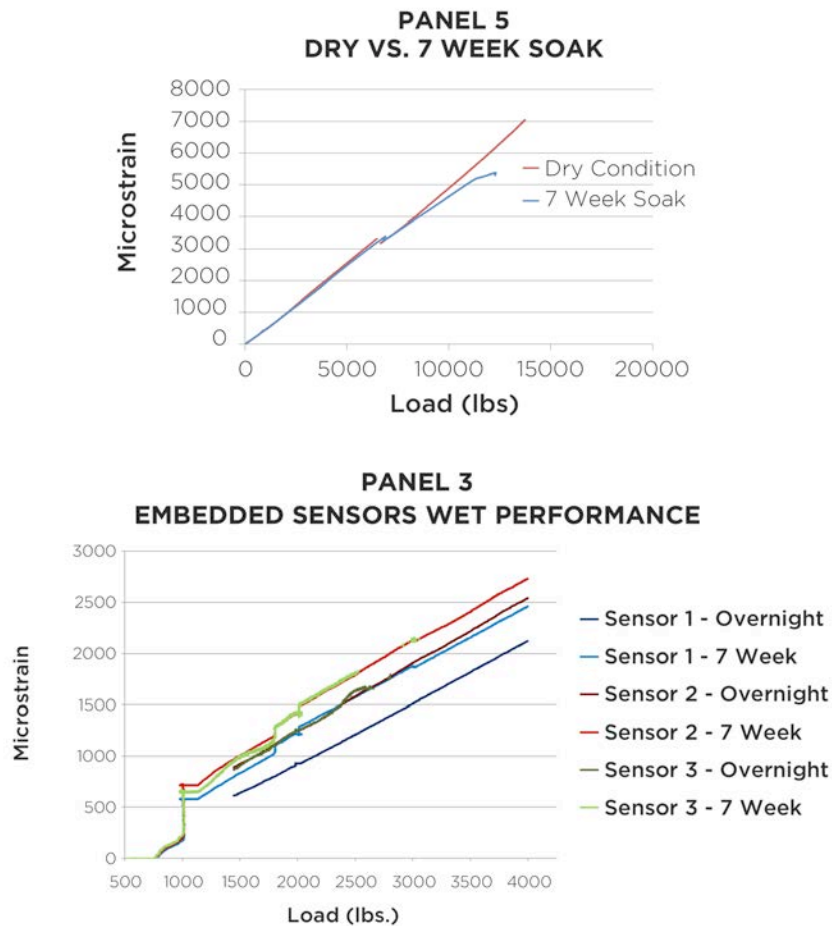
PANEL 3
EMBEDDED SENSORS WET PERFORMANCE

Figure 4: Wet vs dry performance for external sensor (top) and wet performance of embedded sensors (bottom)

Two different panel sensor configurations are presented to demonstrate the performance of the fiber optics in a wet environment. Panel 5 was tested in a dry condition and in two separate wet conditions. The first wet condition involved an overnight soaking in a room temperature water bath, while the second involved an extended soak of 7 weeks. Panel 5 contained one packaged external sensor installed on the surface. Testing was conducted with the sensors located on the tension side of the

beam for this comparison. As shown in Figure 4 (left), there was little change in the sensor performance due to the pre-soak environment. Post-test inspections showed that the epoxy bond of the external sensor to the laminate was starting to wear after 7 weeks in water (recall that non-marine epoxy was used for this application). Panel 3 was selected as an example to demonstrate the performance of internal sensors in a wetted environment. Panel 3 contained three internal sensors located 7 plies from the tension surface and was soaked for the same durations as Panel 5. As shown in Figure 4 (right), no change in performance was noted from a strain response perspective.

PHASE II: OVB AND VARTM

Typical marine platform composite construction uses glass reinforced plastic (GRP) in either a low temperature pre-preg or vacuum assisted resin transfer method (VARTM) manufacturing process. Because of the prevalence of both techniques in marine composite construction, it is important to assess the effect of manufacturing technique on embedded sensor performance. The low temperature GURIT pre-pregs, also referred to as oven vacuum bag (OVB) use a single sided film of epoxy resin on a dry reinforcement, which can be either carbon or glass. To encompass current marine applications, carbon panels were tested similar to the glass panels above to ensure compatibility for use of either reinforcement (carbon may be required to attain stiffness for frequency-driven components). Similarly, VARTM processed material has been proven as a marine environment material. Therefore, test panels were also fabricated using the VARTM method to assess the embedding of FBGs with this process.
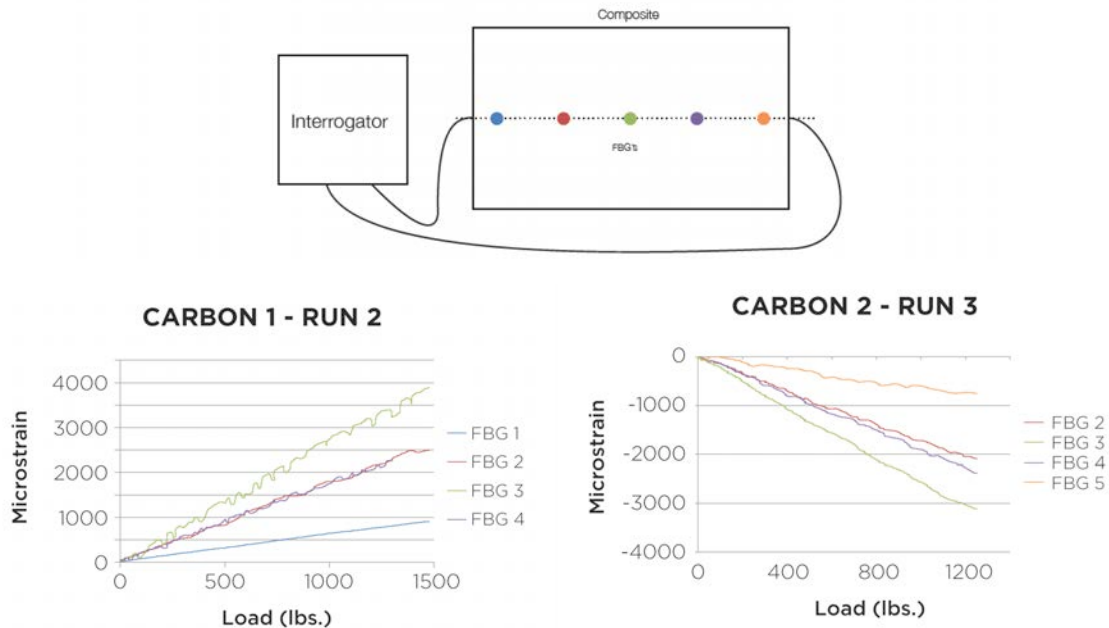

Figure 5: Phase IB test setup (top), Carbon 1 test results (bottom left), Carbon 2 test results (bottom right)

Upon completion of an equivalent 3-pt. bend test as performed in Phase IA, results for the carbon pre-preg were similar to the results of the previous glass pre-preg tests. Figure 5 shows the sensor layout and plotted results for two selected carbon pre-preg panels (Carbon 1 and Carbon 2). These specimens were selected because one was loaded such that the sensors experience tension (Carbon 1) and the other, the sensors experience compression (Carbon 2). It should be noted that 5 FBG sensors were embedded in each panel, but only 4 sensors are plotted. This is because the nominal center wavelength of 1 of the 5 sensors in a standard Micron Optics os1200™ array falls outside of the visible bandwidth of the fiber optic interrogator.
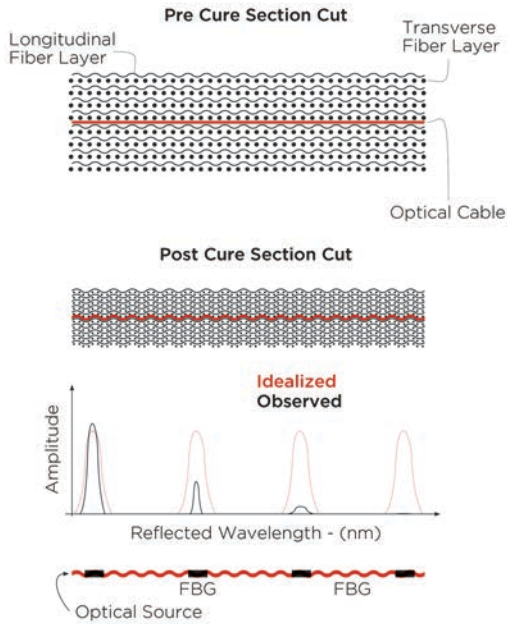
In contrast to the OVB specimens, the VARTM specimens did not perform satisfactorily. Post cure, it was noted that the reflected spectrum, which should reflect 5 distinct sensor peaks, only displayed 1 strong peak and the rest of the peaks fell very close to or below the noise floor altogether. This means that the interrogator is unable to reconcile peak shifts in the spectra, rendering the strain sensor useless. It is believed that this severe attenuation is the result of an acute manifestation of a phenomenon known as micro-bending losses as mentioned earlier. Because of high-frequency undulations in the composite substrate, the optical fiber is subjected to random lateral stresses along the length of the fiber, which impose small radius bends throughout.[21] These small radius bends produce an increased attenuation in the fiber known as micro-bending losses. Micro-bending couples the power from the fundamental guided mode with higher order modes that experience normal scattering and refraction, which in turn, attenuates the global power from the fiber. Figure 6 illustrates the phenomenon. More in depth analysis of bending losses in optical fibers has been performed by other researchers.[22]

In comparing the manufacturing differences between the VARTM and pre-preg panels to better understand the sensor results, a key difference in the processes is that VARTM uses dry reinforcement before introducing resin, thus the dry reinforcement stack introduces more waviness in the surface, causing the fiber optic array to locally bend to conform to the surface. For the pre-preg material with the single side of resin, the vacuum bagging process did not exhibit the same level of surface waviness as the VARTM approach, which appeared to be one of the main drivers of the micro-bending issues.

Figure 6: Micro-bending losses

PHASE II: SHM APPLICATION TO A BOLTED SPECIMEN

This study concludes with a systems-level deployment of an SHM damage detection system with embedded FBGs to detect low levels of connection damage in a fiber-reinforced composite specimen. The damage detection modality employed in this particular experiment is vibration-based (dynamic time histories from the FBG sensors), reflecting a passive sensing scenario in which the monitored structural response is excited by the inherent dynamic loading of the operational environment. There has been significant exploration into defining damage sensitive features in both the time[23-25] and frequency domain[26]. A thorough review of vibration-based damage identification methods has been conducted by Doebling et al.,[27] and Farrar et al.[28]

Test Article Design

Figure 7: Test Article

The test article was designed and fabricated with the same GURIT material system as the previous tests, and with dimensions 18 in. x 10 in. x 3/16 in. thick. Sensors were embedded one ply below the surface in the locations indicated by Figure 7. Sensor configuration and orientation were chosen with the assistance of a finite element model simulating both pre- and post-damage strain fields as well as observing nodal behavior of dynamic strain modes. Sensors 2-4 were oriented diagonally to the local axis of the plate to attempt to capture both "x" and "y" strain component information in a single sensor. Sensors were also installed in non-symmetric locations to ensure the uniqueness of the information captured. An FE model was used to crudely assess which regions of the plate would be most affected by connection damage, and therefore provide insight into potential sensor installation locations. The FE model was subjected to a static tensile loading, and a map of principal stresses was derived from the simulation. Several subsequent runs were completed with a different single bolt removed from the model, and principal stress mappings were generated. Lastly, several difference maps were generated by "subtracting" the simulations with altered boundary conditions from the original simulation with the fully bolted connection. These mappings provided crude insight into how the stress paths would change in the plate with connection damage introduced. Figure 8 illustrates the FE method for generating the difference mappings.
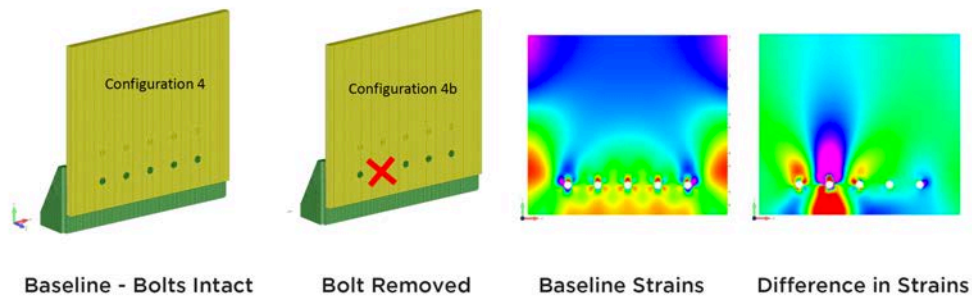
Test Article Fabrication and Sensor Embedment

All sensors for this specimen were installed 1 ply below the top surface of the specimen. Small amounts of resin were used to secure sensors in their designed location, and to route excess optical fiber. As with the previously detailed specimens, great care was taken with the egress of the optical cables to avoid fiber breakage at the egress point. Ongoing research is being conducted to overcome this egress limitation so that further maturation of embedded FBGs for composite SHM can continue[29]. Advancements have been made in multiple methods including bare optical fiber treatment[30], out-of-plane connectors[31], and in-plane connectors[32]. Research of this kind is outside of the scope of this experiment so, although the cured test article itself is robust and durable, the fiber optic leads protruding from the specimen are untreated, fragile and require delicate handling care to mitigate breakage risk. Figure 9 shows the sensors installed before the final ply (left) and after the final ply (right).
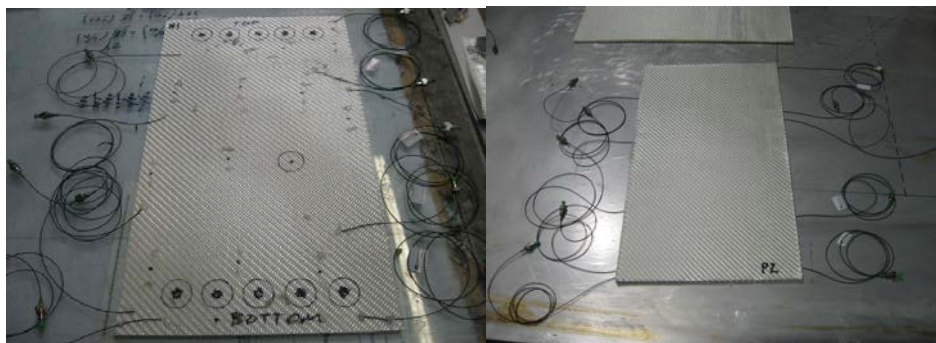

Figure 9: Sensor layout and installation (left) and completed panel ready for cure (right)
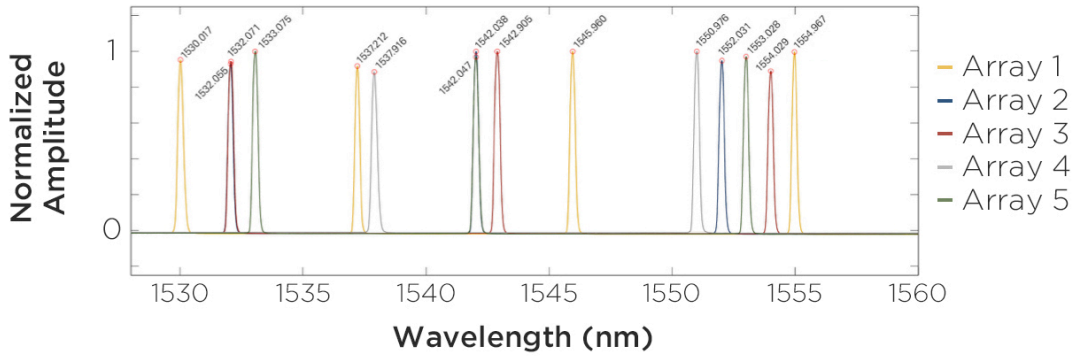
Figure 10: Bragg spectra for all arrays in test article

An important nuance that must be considered in the embedding of fiber optic sensors in composites is that the sensors will be subject to permanent residual strain fields after cure. During the fabrication of the test article it was possible to monitor full FBG spectra before and after the cure. After a vacuum bag was pulled over the part, samples of the Bragg spectra were sampled to establish a baseline spectral shape before the cure. Figure 10 gives a global view of the Bragg spectra peak strength and each sensor's bandwidth allocation within the optical space. Figure 11 then compares Bragg spectra
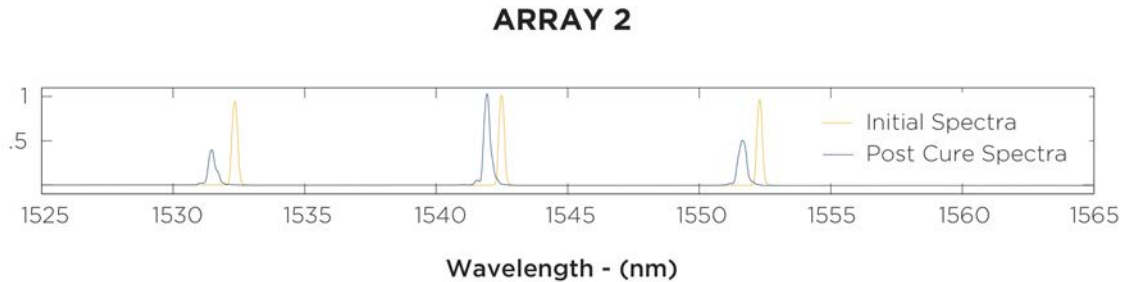

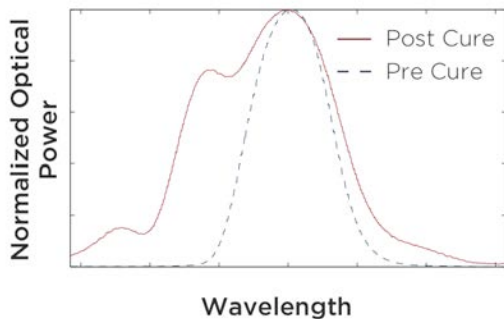Figure 11: Bragg spectra comparison, pre cure vs. post cure

Figure 12: Sensor 7 – pre and post cure

from before and after the cure. There are two observations that can be made from this comparison. First, the cure introduces optical power attenuation that is a direct result of micro-bending losses discussed earlier in the paper. And secondly, the Bragg spectra undergo significant "chirping" during the cure that leads to distorted spectra. This is a contributing cause of the wavelength peak hopping mentioned previously, in which the software loses track of the true Bragg peak wavelength because of the existence of secondary peaks within the spectrum. Remedial techniques to address peak hopping will

be discussed later on in the paper. Figure 12 illustrates the spectral chirping phenomenon by showing the highly symmetric and pronounced peak of the pre-cure Bragg spectrum with the dashed line, compared to a highly distorted Bragg multiple peak post cure with the solid line. The peaks have been normalized and aligned for comparative purposes. This issue of post cure spectral distortion has been the subject of much research[33, 34] and many research and development efforts have been undertaken to develop mitigation strategies.

Testing and Data Acquisition

To validate the damage detection abilities of the embedded sensor network, 90-second strain time histories were recorded for each sensor as the test article was actuated by band-limited white noise (10-1000 Hz) transversely with an electro-dynamic shaker, intended to simulate a pseudo-random dynamic operating environment. In between each time record, connection damage was accumulated in the structure by axially loading the part with increasing loads. Finally, the part was transversely loaded with an actuator to introduce damage in a location other than the connection. Figure 13 (left) shows the test article installed in the test fixture. A Micron Optics SM170 Fiber Optic Interrogator was used as both the broadband light source and light receiver, and Enlight, a proprietary Micron Optics software program, was used to do wavelength peak tracking at a sampling rate of 2000Hz. A 50 lb. MB Dynamics™ electro-mechanical shaker that was powered by a MB Dynamics™ SL500VCF power amplifier actuated the structure transversely. Data was collected with a National Instruments™ cDAQ-9178 data acquisition system.

Figure 13: Testing equipment (right) and test setup (left)

It is important to understand the damage progression experienced in the connection of the specimen as a result of the loading, between the vibration testing, but without removing the test specimen from the fixture after each loading. This was accomplished by loading a surrogate panel with no sensors and monitoring the incremental progression of damage.

The assumption is then made that the part outfitted with the sensor arrays will

experience the same progression of damage. Figure 14 shows the connection damage introduced by the incremental loading. From this figure, one can see that at 40,000 lb. the load could not be sustained by the test specimen and it began to deform plastically in a

Figure 14: Bearing damage observations: (far left) after 10,000 lb. load, no visible damage; (center left) after 20,000 lb. load, slight bearing damage; (center right) after 30,000 lb, significant bearing damage, and (far right) critical bearing damage and severe specimen elongation.

bolt shear out mode. Therefore, loading was terminated when the part experienced ~0.5 in. of total elongation. The dynamic data run performed after each static load increment lasted 90 seconds, and the first 5 seconds of the time histories were windowed off to account for transient effects and inconsistencies in the start of the (uncontrolled) shaker input. The 85-second time history was then segmented into 3-second subsections that make up individual "tests." Given the sampling rate of the interrogator, (2000 Hz) the number of samples in each test was 6000. There were thus 28 total tests for each case, baseline, undamaged, damage level 1, damage level 2, damage level 3, damage level 4, and the transversely loaded case, making 196 total tests. The complete test matrix is found in Table 1.

Table 1: Test Matrix

Testing Procedure	
Structural State	**Action**
Baseline	None
Undamaged	None
Damage Level 1	Load to 10,000 lbs. then return to zero
Damage Level 2	Load to 20,000 lbs. then return to zero
Damage Level 3	Load to 30,000 lbs. then return to zero
Damage Level 4	Load to 40,000 lbs. then return to zero
Damage Level 5	Transversely loaded until severe matrix cracking was visible.

Wavelength Hopping Correction

As mentioned previously in the paper, peak hopping or wavelength hopping is a challenge that may need to be overcome when tracking highly dynamic strains with FBGs that are chirped from embedment. In this study, the raw acquired data showed

significant dropouts from multiple sensors which would require correction before further processing could be performed. Auto-regression (AR) was employed to correct for lost data points. An *n*-th order AR model assumes that a current point in time can be modeled as a linear combination of *n* previous points[17]

$$x(t) = \sum_{j=1}^{n} a_n x(t-j) + e(t) \tag{1}$$

where *x(t)* = the signal at time t, a_n = the AR coefficients and *e(t)* = the error term. Typically, the AR model order needs to be chosen such that the full structure of a signal is modeled without over fitting to the noise in the system. This ensures that the model is representative of the system response holistically and not simply a copy of a particular instance of a response. In this application, the AR model is expected to fit as closely to a particular signal as possible so the model order, *n*, was chosen to be as large as possible between sensor dropouts. Figures 15 and 16 illustrate the implementation of auto regression as a corrective technique for wavelength hopping. Using the AR model, the frequency content of the corrected time histories will be preserved better than if a simple averaging method were used, or if the missing values were just assumed to be zero.
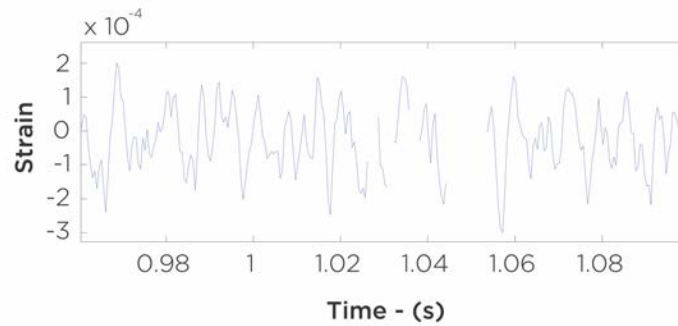
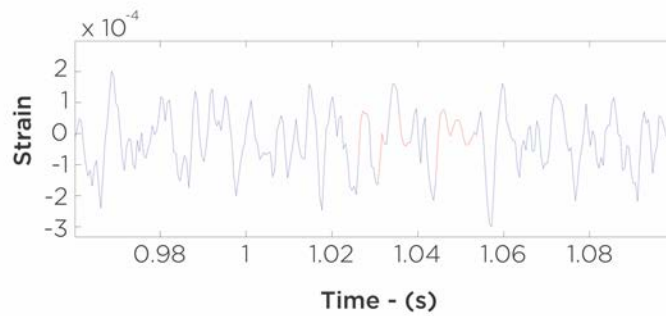Figure 15: Raw time history with significant wavelength hopping

Figure 16: Time history corrected via an AR model

Damage Sensitive Feature Extraction – Frequency Domain

Damage is generally defined as changes to the material and/or geometric properties of the structure such that the structure's intended performance is adversely

affected. These changes are often observed as stiffness losses and can be detected in the frequency response of the structure.

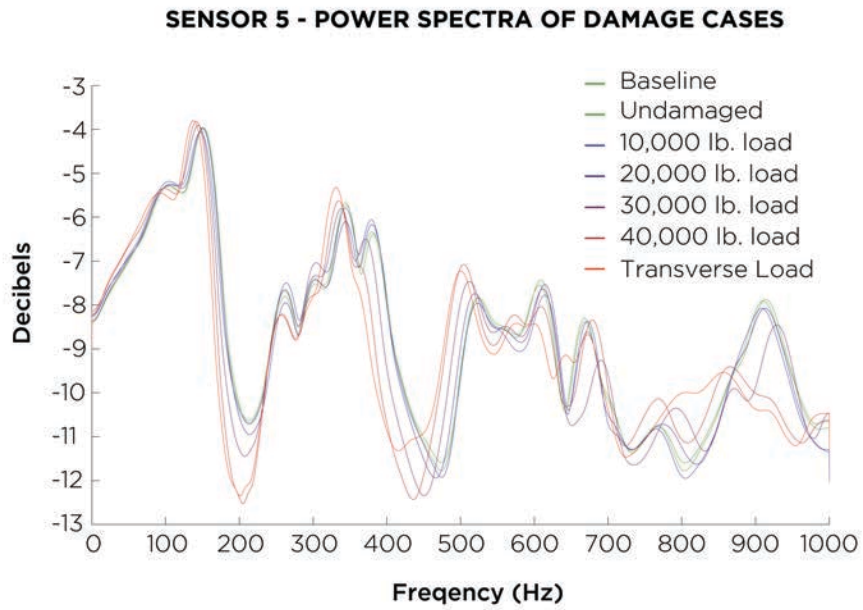**SENSOR 5 - POWER SPECTRA OF DAMAGE CASES**

Figure 17: Power spectra from sensor 5 for all damage states

Figure 17 shows typical power spectra for a given sensor over all damage levels. Figure 18 shows a normalized view of one of the peaks. A clear progressive shift towards lower frequencies can be observed as damage accumulates in the structure.
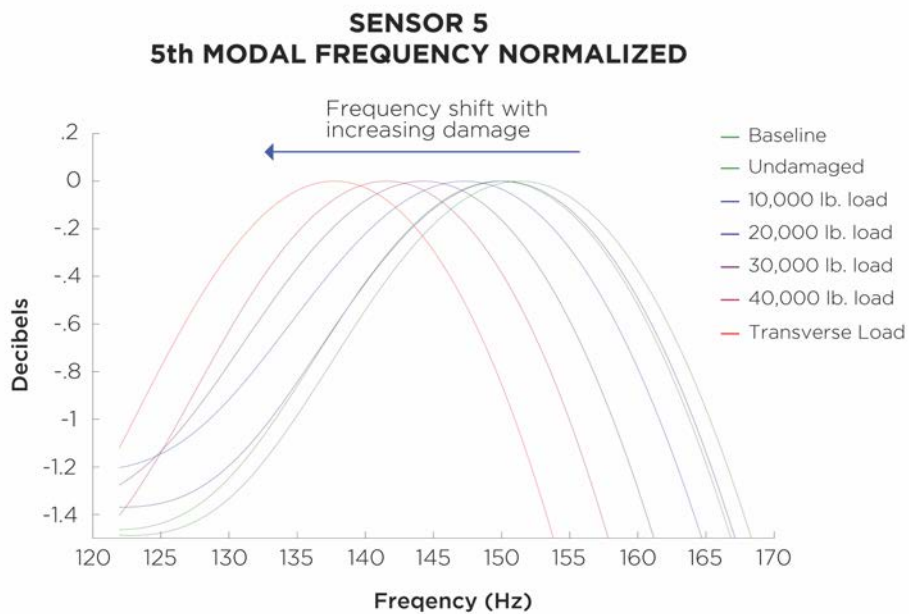
SENSOR 5
5th MODAL FREQUENCY NORMALIZED

Figure 18: Normalized power spectra for sensor 5 – 5th mode

The chosen damage sensitive feature, then, is a vector of frequencies that correspond to peaks in the power spectral density of the signal:

$$X = [\Delta_1 \; \Delta_2 \; ... \; \Delta_j] = \left[argmax \left(\widehat{S_u}(\omega_{baseline,j}) \right) \right]^T \tag{2}$$

where $\widehat{S_u}$ corresponds to the power spectral density of a time history in an unknown structural state, computed via the Welch method[35], and $\omega_{baseline,j}$ corresponds to the jth peak observed in the power spectral density of the baseline state as the arithmetic mean of all baseline tests. The entire spectra from 0-1000 Hz (Nyquist) was searched for peaks to form the initial set of baseline frequencies. Δ_j, then, is given by Equation 3,

$$\Delta_j = \omega_{baseline,j} - \omega_{damaged,j} \tag{3}$$

where $\omega_{damaged,j}$ is a local maximum of $\widehat{S_u}$ in the same frequency range as the baseline peak, $\omega_{baseline,j}$. In many cases, $\widehat{S_u}(\omega_{baseline,j})$ does not contain a local maximum within a window centered around $\omega_{baseline,j}$. In such instances, that particular peak was omitted from X. So the dimension of X is dictated by the number of peaks found in common between the baseline and all structural states within given windows defined by the nearness of sequential local maxima of the baseline spectrum. The dimension of the multivariate feature vector is then reduced to a scalar damage sensitive feature using the Mahalanobis squared distance given by,

$$D_i = (X_i - \bar{X})^T \Sigma^{-1} (X_i - \bar{X}) \tag{4}$$

where X_i is the feature vector from an unknown structural state, $\bar{X}$ is the mean vector of training data set, and Σ is the covariance matrix of the training set, where the training set is the ensemble of 28 baseline time histories. This feature will be used to determine discordant outliers from the data sets[5] and thus can be used to indicate a damaged structural state. Figure 19 displays representative test data from 3 of the sensors.
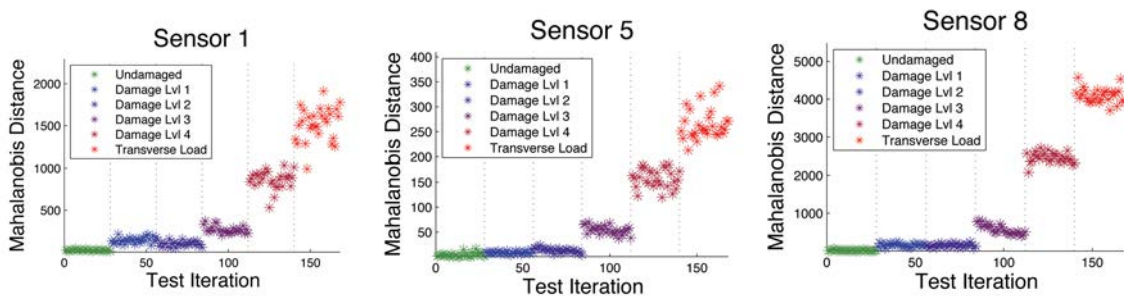

Figure 19: (left) Sensor 8 Mahalanobis distance scatter plot; (center) Sensor 3 Mahalanobis distance scatter plot; (right) Sensor 10 Mahalanobis distance scatter plot;

Relatively stable Mahalanobis distances are observed until damage Level 3 (after 30,000 lb. axial load.), which is consistent with the damage observed in the surrogate panel without sensors (Figure 14). Low variance is also observed between tests at the same damage levels, which provides promise for the success of deviation-based hypothesis testing to be discussed later in the paper.

Damage Sensitive Feature Extraction – Time Domain

As previously mentioned, auto regressive (AR) models (1) predict a function value at a particular point in time as a linear combination of n past values, where n is the model order. In application to structural health monitoring, if a numerical model is generated from the structure in a known healthy state, then the ability of that model to predict accurately should decay with damage accumulation. A monotonic error calculation of the error term such as root mean squared (RMS) or square root sum of the squares (SRSS) can be used as a damage sensitive feature. For this study, the AR model coefficients, a_i, themselves will be a damage sensitive feature vector.

For each test signal, the coefficients of a 27th order AR model were generated using linear predictive coding in MATLAB™. An AR order optimization algorithm employing Bayesian Information Criterion (BIC) was used, and the optimum AR order for the signal ensemble was 39. Because only 28 baseline signals comprise the Mahalanobis distance sample set, the second dimension is limited to being 27. Figure 20 presents representative test data from sensors 2, 5, and 8.
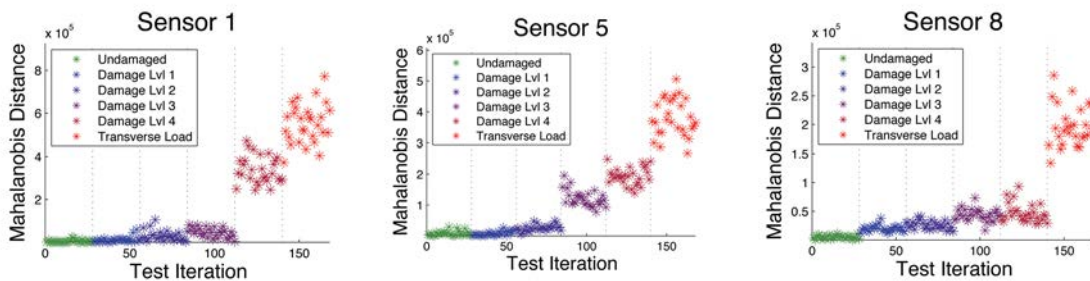

Figure 20: Mahalanobis distance of AR coefficients for (left) sensor 2; (center) sensor 5; and (right) sensor 8

The time domain feature produces similar results to the frequency domain. The additional variance among the tests of congruent damage levels is likely due to high variability in signal to noise ratios among the sensors, which does not get "averaged out" as it does in the frequency domain.

Hypothesis Testing

Outlier observation via the Mahalanobis distance metric has been shown to be a potentially powerful discriminator ("detector") of damage, but fundamentally a quantitative statistical treatment must be employed to rigorously answer the question of whether the distance metric has changed in a statistically significant way as to indicate

damage. This question is answered by hypothesis testing, and specifically, binary hypothesis testing: "Is the structure critically damaged or not?".

Thus, the question relies on a definition of criticality, which is always application-dependent. In this experiment, the 20,000 lb. load level (damage level 2) began to introduce visible damage but it was not until the 30,000 lb. load was applied that damage was observed that would warrant significant concern in a structural sense. In order to test the Mahalanobis-distance-based detector, a random sample of data is collected from all undamaged cases. Recall that this would be made up of the baseline, damage level 1, and damage level 2 tests, 84 tests in all. The training set is comprised of a random selection of 42 of these undamaged tests. Probability density functions (PDFs) for each sensor in the training set are constructed (Figure 22) and are tested that they follow Gaussian distributions via a Kolmogorov-Smirnov test[36]. It should be noted that although deviations in normality for this experiment were sufficiently small to not violate the Kolmogorov-Smirnov test, this might not always be the case. Such situations would merit employment of density methods or auto associative networks.[37]

After the training set construction, the testing set is comprised of all tests from critically damaged cases (damage level 3-5) and the remaining undamaged tests not used to construct the training set. A simple discordancy test will be used to identify outliers and make decisions about the structural state according to Equation (5)[38], where z_i is the outlier index, d_i is the Mahalanobis distance value being tested, and μ and σ are the mean and standard deviation of Mahalanobis distances of the baseline set for a particular sensor:

$$z_i = \frac{d_i - \mu}{\sigma} \tag{5}$$

The test itself is performed according to the binary hypothesis test according to Equation (6).

$$H_o : z_i < 3 \text{ (null-healthy structure)}$$
$$H_1 : z_i \geq 3 \text{ (alternative-damaged structure)} \tag{6}$$

For each test statistic that rejects the null hypothesis, one can say with 99.7% confidence (3 standard deviations under reasonably assumed normal statistical structure from central limit theorem implications) that it does not represent a feature from the damage case.

All test data were randomly permutated, and the aforementioned hypothesis test was performed on each test statistic for each sensor. For the first test, a target of 50% sensor agreement among all sensors (simple sensor fusion voting) for a damaged diagnosis is required. The results are presented in Figure 23.
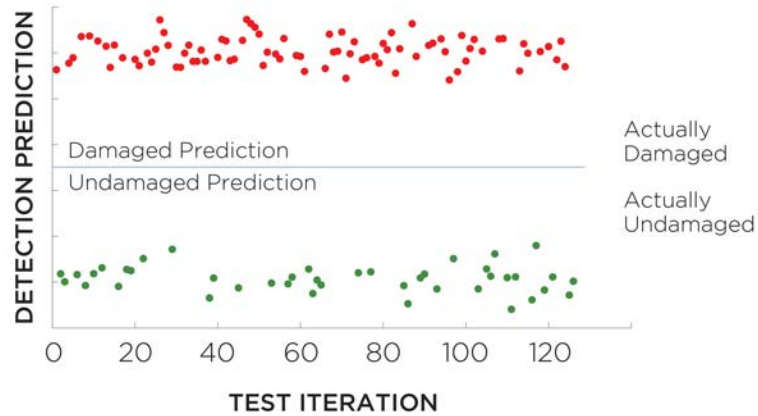
Figure 21: Binary hypothesis test results: 50% sensor agreement. Red and green represent true structural state and y-axis value represents predicted state with 0 being an undamaged prediction and 1 being a damaged prediction

For this test, 100% agreement between the predicted structural state and the actual structural state is observed (due to the finite data set; in reality, 100% wouldn't be observed over the structural lifetime, but the point is that the number is very close to the 99.7% target).

For the second experiment, decision-cost penalties are introduced. For structures whose failure could result in loss of life, a false negative could lead to catastrophic failure if actual damage is not addressed. A false positive would only cost the intended maintenance time or, more severely, prescribed down time of the structure that is not actually necessary. For many applications, it is highly likely that the consequence of a false negative far outweighs the cost of a false positive, so the requirement is modified to require only 15% sensor agreement. This means that if any two sensors of the twelve agree that a particular test statistic does not come from the undamaged PDF, a damage diagnosis will be given. Figure 24 presents the results from this experiment, and a 96.8% correct prediction rate with 4 false positives was observed, which have been indicated with circles.
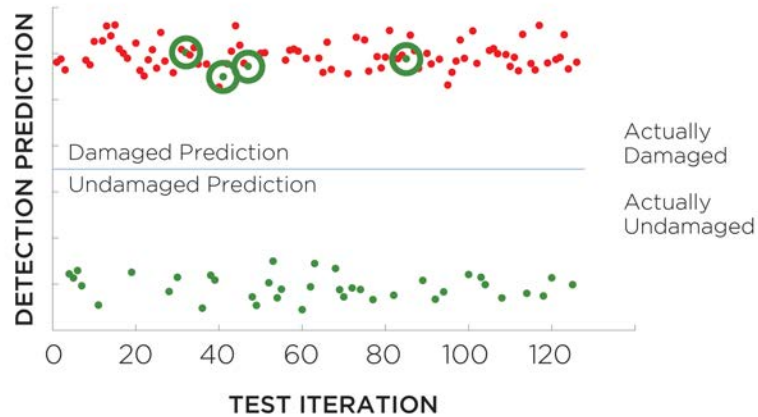

Figure 22: Binary hypothesis test results: 15% sensor agreement. Red and green represent true structural state and y-axis value represents predicted state with 0 being an undamaged prediction and 1 being a damaged prediction

CONCLUSIONS

In this study, several composite specimens (of two types) were constructed with embedded and surface mounted fiber Bragg gratings to study (1) the effects of the embedding process on the FBGs; (2) the FBG performance in wet vs. dry environments, and (3) how an SHM solution performed on detecting composite bolt bearing damage in a progressive loading test.

For (1), the sensors survived the curing process (185°F up to 12 hours) and were generally useable afterwards for testing. However, micro-bending and micro-constriction in some cases caused both a reduced signal-to-noise ratio in the reflected power at the central wavelength as well as chirping of the spectrum. This effect was particularly severe in the case of the VARTM manufacturing process. This led to reduced performance in central wavelength peak-tracking, causing false discontinuities in the strain response; this was shown to be correctable, in a reasonable way, using linear predictive coding. For (2), overnight soaking of surface and embedded sensors showed no degradation, but the non-marine epoxy did show signs of degradation after the 7-week immersion. The internal sensors' performance was not affected at all over the 7 weeks. Finally, in (3) it was demonstrated that as connection bearing damage is incrementally introduced into by loading, damage-sensitive features may be extracted from the strain time histories in both the frequency domain (power spectral densities) and the time domain (auto-regressive models). Then these features were successfully implemented in binary hypothesis testing in order to assess performance at "blindly" detecting the damage.

REFERENCES

1. Mouritz, A. P., et al. "Review of advanced composite structures for naval ships and submarines." *Composite structures* 53.1 (2001): 21-42.

2. Cao, Jun, and Joachim L. Grenestedt. "Design and testing of joints for composite sandwich/steel hybrid ship hulls." *Composites Part A: Applied science and manufacturing* 35.9 (2004): 1091-1105.

3. Farrar, Charles R., et al. *A review of structural health monitoring literature: 1996-2001*. Los Alamos, NM: Los Alamos National Laboratory, 2004.

4. Staszewski, Wieslaw, Christian Boller, and Geoffrey R. Tomlinson, eds. *Health monitoring of aerospace structures: smart sensor technologies and signal processing*. John Wiley & Sons, 2004.

5. Chang, Fu-Kuo, and Kuo-Yen Chang. "A progressive damage model for laminated composites containing stress concentrations." *Journal of Composite Materials* 21.9 (1987): 834-855.

6. Choi, Hyung Yun, and Fu-Kuo Chang. "A model for predicting damage in graphite/epoxy laminated composites resulting from low-velocity point impact." *Journal of composite materials* 26.14 (1992): 2134-2169.

7. Ladeveze, Pierre, and E. LeDantec. "Damage modelling of the elementary ply for laminated composites." *Composites Science and Technology* 43.3 (1992): 257-267.

8. Hung, Chang-Li, and Fu-Kuo Chang. "Bearing failure of bolted composite joints. Part II: model and verification." *Journal of Composite Materials* 30.12 (1996): 1359-1400.

9. Abrate, Serge. "Modeling of impacts on composite structures." *Composite structures* 51.2 (2001): 129-138.

10. Alfano, G., and M. A. Crisfield. "Finite element interface models for the delamination analysis of laminated composites: mechanical and computational issues." *International journal for numerical methods in engineering* 50.7 (2001): 1701-1736.

11. Farrar, Charles R., and Keith Worden. "An introduction to structural health monitoring." *Philosophical Transactions of the Royal Society of London A: Mathematical, Physical and Engineering Sciences* 365.1851 (2007): 303-315.

12. Winkelmann, Charles, Wahyu Lestari, and Valeria La Saponara. "Composite structural health monitoring through use of embedded PZT sensors." *Journal of Intelligent Material Systems and Structures* (2011): 1045389X11406303.

13. Kessler, Seth S., et al. "Damage detection in composite materials using frequency response methods." *Composites Part B: Engineering* 33.1 (2002): 87-95.

14. Haynes, Colin, et al. "Monitoring of bearing failure in composite bolted connections using ultrasonic guided waves: A parametric study." *Structural Health Monitoring* 13.1 (2014): 94-105.

15. Qiao, Pizhong, et al. "Curvature mode shape-based damage detection in composite laminated plates." *Composite Structures* 80.3 (2007): 409-428.

16. Kessler, Seth S., S. Mark Spearing, and Constantinos Soutis. "Damage detection in composite materials using Lamb wave methods." *Smart Materials and Structures* 11.2 (2002): 269.

17. Kersey, Alan D., et al. "Fiber grating sensors." *Journal of lightwave technology* 15.8 (1997): 1442-1463.

18. De Oliveira, R., C. A. Ramos, and A. T. Marques. "Health monitoring of composite structures by embedded FBG and interferometric Fabry–Pérot sensors." *Computers & structures* 86.3 (2008): 340-346.

19. Majumder, Mousumi, et al. "Fibre Bragg gratings in structural health monitoring—Present status and applications." *Sensors and Actuators A: Physical* 147.1 (2008): 150-164.

20. Peters, Kara. "Full-spectrum FBG analysis of inhomogeneous, fast-varying strain effects." *Asia Pacific Optical Sensors Conference*. International Society for Optics and Photonics, 2012.

21. Di Sante, R., and L. Donati. "Strain monitoring with embedded Fiber Bragg Gratings in advanced composite structures for nautical applications." *Measurement* 46.7 (2013): 2118-2126.

22. Arya, Vivek, et al. "Microbend losses in singlemode optical fibers: theoretical and experimental investigation." *Journal of lightwave technology* 13.10 (1995): 1998-2002.

23. Sohn, Hoon, and Charles R. Farrar. "Damage diagnosis using time series analysis of vibration signals." *Smart materials and structures* 10.3 (2001): 446.

24. Sohn, Hoon, et al. *Applying the LANL statistical pattern recognition paradigm for structural health monitoring to data from a surface-effect fast patrol boat*. No. LA-13761-MS. Los Alamos National Lab., NM (US), 2001.

25. Gul, Mustafa, and F. Necati Catbas. "Statistical pattern recognition for Structural Health Monitoring using time series modeling: Theory and experimental verifications." *Mechanical Systems and Signal Processing* 23.7 (2009): 2192-2204.

26. Fan, Wei, and Pizhong Qiao. "Vibration-based damage identification methods: a review and comparative study." *Structural Health Monitoring* 10.1 (2011): 83-111.

27. Doebling, Scott W., et al. *Damage identification and health monitoring of structural and mechanical systems from changes in their vibration characteristics: a literature review*. No. LA--13070-MS. Los Alamos National Lab., NM (United States), 1996.

28. Farrar, Charles R., et al. *A review of structural health monitoring literature: 1996-2001*. Los Alamos, NM: Los Alamos National Laboratory, 2004.

29. Kinet, Damien, et al. "Fiber Bragg grating sensors toward structural health monitoring in composite materials: Challenges and solutions." *Sensors* 14.4 (2014): 7394-7419.

30. Kinet, Damien, et al. "Behaviour of optical fibre Bragg grating sensors embedded into composite material under flexion." *Proceedings of the 14th European conference on composite materials*. 2010.

31. Beukema, R. P. "Embedding technologies of FBG sensors in composites: Technologies, applications and practical use." *Proceedings of the 6th European Workshop on Structural Health Monitoring*. 2012.

32. Kang, H. K., et al. "Development of fibre optic ingress/egress methods for smart composite structures." *Smart materials and structures* 9.2 (2000): 149.

33. Kuang, KSCea, et al. "Embedded fibre Bragg grating sensors in advanced composite materials." Composites Science and Technology 61.10 (2001): 1379-1387.

34. Luyckx, Geert, et al. "Strain measurements of composite laminates with embedded fibre Bragg gratings: Criticism and opportunities for research."Sensors 11.1 (2010): 384-408.

35. Welch, Peter D. "The use of fast Fourier transform for the estimation of power spectra: A method based on time averaging over short, modified periodograms." *IEEE Transactions on audio and electroacoustics* 15.2 (1967): 70-73.

36. Chakravarti, Indra Mohan, and Radha G. Laha. "Handbook of methods of applied statistics." *Handbook of methods of applied statistics*. John Wiley & Sons, 1967.

37. Farrar, Charles R., et al. "Integrated structural health monitoring." 6th Annual International Symposium on NDE for Health Monitoring and Diagnostics. International Society for Optics and Photonics, 2001.

38. Sohn, Hoon, et al. "Structural health monitoring using statistical pattern recognition techniques." *Journal of dynamic systems, measurement, and control* 123.4 (2001): 706-711.